J. Fluid Mech. (1980), *vol.* 98, *part* 2, *pp.* 397–416
Printed in Great Britain

Oscillatory flow in curved pipes. Part 2. The fully developed case

By T. MULLIN† AND C. A. GREATED
Department of Physics, University of Edinburgh

(Received 4 April 1979)

A theoretical and experimental investigation of oscillatory flow in curved pipes is presented. The equations for fully developed laminar flow are found to depend on an amplitude parameter G and a frequency parameter α. Initially the Navier–Stokes equations are expanded in terms of G and the resulting linearized equations are solved numerically using finite Hankel integral transforms. A further expansion is used for the case $\alpha \to 0$ and closed-form solutions are presented.

Laser-Doppler anemometry has been used to obtain velocity information in oscillatory air flow in small-diameter curved glass tubes. Using this technique, low-Reynolds-number experiments were carried out and comparison between theory and experiments is presented.

For $\alpha \leqslant 1$ the velocity distributions found are essentially those for steady flow, while for $\alpha \geqslant 11{\cdot}0$ the results are not at variance with earlier work. It is for the transition stage between these two regimes that unexpected behaviour is recorded, but a satisfactory explanation is found in terms of general trends within the flow.

1. Introduction

There has been a considerable amount of research into steady flow in curved pipes but it is only recently that the problem of unsteady flow has been considered. The first theoretical study of oscillatory flow in a curved pipe was carried out by Lyne (1970) who used boundary-layer approximations to solve the linearized Navier–Stokes equations for large values of the frequency parameter $\alpha = a(\omega/\nu)^{\frac{1}{2}}$. His solutions are valid for the cases $R_s \ll 1$ and $R_s \gg 1$, where $R_s = K^2a/(R\nu\omega^3)$ is the Reynolds number of the steady secondary-flow component. Here K is the amplitude of the applied pressure gradient, a the radius of the pipe, R the radius of curvature of the bend, ν is the kinematic viscosity and ω the radial frequency of the flow.

The main result of Lyne's work was to show the existence of a four-vortex secondary-flow system. The secondary flow in the central core of the tube was found to be steady and directed from the outside of the curve to the inside, i.e. in the opposite sense to that for steady flow. Around the walls of the pipe the secondary vortex was directed in the same sense as that for steady flow. Lyne postulated that for $\alpha \leqslant 12{\cdot}9$ the normal two-vortex system would persist as found in the steady-flow work of Dean (1927, 1928).

Lyne's findings were verified experimentally by Bertelsen (1975) and Munsen (1975, 1976). They investigated the nature of the steady secondary-flow component

† Present address: Mathematical Institute, University of Oxford.

0022–1120/80/4483–1040 $02.00

using flow-visualization techniques. There is good agreement between their experimentally determined α value for the transition of the two-vortex to the four-vortex system and the theoretical value given by Lyne.

However, Bertelsen found that there is a distortion of the outer vortices which is not predicted by the theory of Lyne. His experiments were carried out in a U-tube of curvature 0·1 and since the theory is strictly valid only for very small curvature he has considered the effects of finite curvature on the equations of Lyne, in Bertelsen (1974).

The agreement between theory and experiment is improved but the analysis requires that the axial velocity distribution is such that its maximum occurs towards the inside of the curve at all phase positions in the pressure cycle. No comment is made upon this by Bertelsen but it is clear that a completely different flow situation exists in the high-frequency limit to that found for steady flow.

Another attempt at solving the Navier–Stokes equations for this problem was made by Zalosh & Nelson (1972). Their analysis consisted of linearizing the Navier–Stokes equations by expanding them in powers of the curvature, which is assumed small, and solving the resulting equations using numerical techniques. The results ought to be valid for all values of α but restricted to the limit $R_s \ll 1$. Further, closed-form solutions were obtained in the limits $\alpha \to 0$ and $\alpha \to \infty$.

Zalosh & Nelson's work relies heavily on the thesis of Zalosh (1970) and unfortunately within the thesis there is a major error in the derivation of the third-momentum equation. This gives a completely wrong axial velocity distribution for the curved pipe. Further, there is an error in the use of the integral transform for the first-order secondary-flow equation which gives too low an α value for the transition of the two-vortex to the four-vortex system. The paper presented by Zalosh & Nelson contains the correct equations but the results which are presented therein appear to be inconsistent with these.

A more general approach to the problem is presented by Blennerhassett (1976) and Smith (1975) who considered the case of an oscillatory pressure gradient superimposed on a mean. This introduces a third parameter into the small-curvature equations, viz. the steady-flow Dean number. The interplay between the oscillatory part and the mean part of the flow was found to be complicated with the two types of secondary-flow generation found. There was inward centrifuging generated by the boundary conditions of the oscillatory flow and outward centrifuging caused by centrifugal effects of the steady flow. In the oscillatory limit, however, agreement was found with Lyne for large values of α and with Dean in the quasi-steady limit. Also Blennerhassett found the centre of axial-velocity distribution for the oscillatory component to be displaced towards the inside of the curve, and attributed this to the reverse secondary flow.

In this study we are considering the case of viscous, incompressible, laminar flow in a torus under the action of a pressure gradient $K \cos \omega t$. The equations are linearized by expanding in terms of an amplitude parameter G and the resulting equations are solved using finite Hankel integral transforms. The solutions are valid for all values of the frequency parameter α with the restriction $R_s \ll 1$. Closed-form solutions are obtained in the quasi-steady limit by a further expansion in α^2 to aid physical insight into the problem.

Finally, theory and experiment are compared and it is shown that many of the main flow features are present in the first-order theoretical approximations.

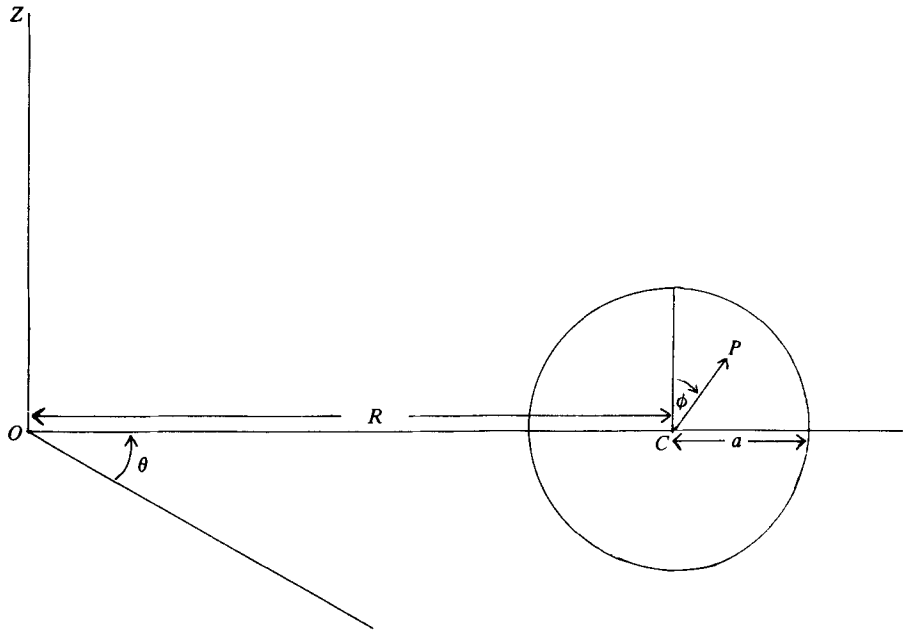

FIGURE 1. Co-ordinate system.

2. The equations of motion

The system of co-ordinates used is shown in figure 1. A circular pipe of radius a is coiled in a toroid around an axis OZ such that a section of the pipe is specified by an axial plane through the pipe which makes an angle θ to the fixed axial plane. The radius of the circle in which the pipe is coiled is given by R and this will be used to specify the non-dimensional radius of curvature (a/R), which will be assumed small in this analysis.

Any point Q within a plane of the pipe will be specified by the orthogonal co-ordinates (r', ϕ, θ) and the components of velocity corresponding to these co-ordinates will be given by U', V' and W' respectively. Fully developed flow will be assumed to exist in the plane of interest and thus U', V' and W' will be independent of θ, but P the pressure will not be.

The small-curvature unsteady-flow equations may be obtained directly from the steady-flow equations of Dean (1928):

$$\frac{\partial U'}{\partial t}+U'\frac{\partial U'}{\partial r'}+\frac{V'}{r'}\frac{\partial U'}{\partial \phi}-\frac{V'^2}{r'}-\frac{W'^2\sin\phi}{R}=-\frac{\partial}{\partial r'}\left(\frac{P}{l}\right)-\frac{\nu}{r'}\frac{\partial}{\partial \phi}\left(\frac{\partial V'}{\partial r'}+\frac{V'}{r'}-\frac{1}{r'}\frac{\partial U'}{\partial \phi}\right); \tag{2.1}$$

$$\frac{\partial V'}{\partial t}+U'\frac{\partial V'}{\partial r'}+\frac{V'}{r'}\frac{\partial U'}{\partial \phi}+\frac{U'V'}{r'}-\frac{W'^2\cos\phi}{R}=-\frac{1}{r'}\frac{\partial}{\partial \phi}\left(\frac{P}{l}\right)+\nu\frac{\partial}{\partial r'}\left(\frac{\partial V'}{\partial r'}+\frac{V'}{r'}-\frac{1}{r'}\frac{\partial U'}{\partial \phi}\right); \tag{2.2}$$

$$\frac{\partial W'}{\partial t}+U'\frac{\partial W'}{\partial r'}+\frac{V'}{r'}\frac{\partial W'}{\partial \phi}=-\frac{1}{R}\frac{\partial}{\partial \theta}\left(\frac{P}{l}\right)+\nu\nabla'^2W'; \tag{2.3}$$

$$\frac{\partial U'}{\partial r'}+\frac{U'}{r'}+\frac{1}{r'}\frac{\partial U'}{\partial \phi}=0. \tag{2.4}$$

Here $$\nabla'^2 \equiv \frac{\partial^2}{\partial r'^2} + \frac{1}{r'}\frac{\partial}{\partial r'} + \frac{1}{r'^2}\frac{\partial^2}{\partial \phi^2},$$

ν is the kinematic viscosity of the fluid and l its density. From the equation of continuity (2.4), the stream function $f(r', \phi)$ can be introduced such that

$$U' = -\frac{1}{r'}\frac{\partial f}{\partial \phi}, \quad V' = \frac{\partial f}{\partial r'}. \tag{2.5}$$

Also the pressure terms can be eliminated between equations (2.1) and (2.2) and the vorticity equation for flow in the cross-section obtained, such that

$$-r'\frac{\partial}{\partial t}(\nabla'^2 f) + \left(\frac{\partial f}{\partial \phi}\frac{\partial}{\partial r'} - \frac{\partial f}{\partial r'}\frac{\partial}{\partial \phi}\right)\nabla'^2 f + \frac{2W'}{r'}\left(r'\cos\phi\frac{\partial W'}{\partial r'} - \sin\phi\frac{\partial W'}{\partial \phi}\right) = -\nu r'\nabla'^4 f, \tag{2.6}$$

$$\frac{\partial W'}{\partial t} + \frac{1}{r'}\left(\frac{\partial f}{\partial r'}\frac{\partial W'}{\partial \phi} - \frac{\partial f}{\partial \phi}\frac{\partial W'}{\partial r'}\right) = -\frac{1}{R}\frac{\partial}{\partial \theta}\left(\frac{P}{l}\right) + \nu\nabla'^2 W'. \tag{2.7}$$

A sinusoidal pressure gradient which has no mean part is imposed on the flow such that

$$-\frac{1}{R}\frac{\partial}{\partial \theta}\left(\frac{P}{l}\right) = K\cos\omega t, \tag{2.8}$$

where K is the amplitude of the applied pressure gradient and ω is the angular frequency.

Using the following non-dimensionalization a more convenient form of the equation is found:

$$r = \frac{r'}{a}, \quad \tau = \omega t, \quad \Psi = \frac{f}{\nu}, \quad w = \frac{W'\omega}{K}.$$

Equation (2.6) becomes

$$\frac{a^2\omega}{\nu}\frac{\partial}{\partial \tau}(\nabla^2\Psi) - \frac{1}{r}\left(\frac{\partial \Psi}{\partial \phi}\frac{\partial}{\partial r} - \frac{\partial \Psi}{\partial r}\frac{\partial}{\partial \phi}\right)\nabla^2\Psi - \frac{2K^2a^3}{R\nu^2\omega^2}\frac{w}{r}\left(r\cos\phi\frac{\partial w}{\partial r} - \sin\phi\frac{\partial w}{\partial \phi}\right) = \nabla^4\Psi, \tag{2.9}$$

where $$\nabla^2 \equiv a^2\nabla'^2;$$

and equation (2.7) becomes

$$\frac{a^2\omega}{\nu}\frac{\partial w}{\partial \tau} + \frac{1}{r}\left(\frac{\partial \Psi}{\partial r}\frac{\partial w}{\partial \phi} - \frac{\partial \Psi}{\partial \phi}\frac{\partial w}{\partial r}\right) = \frac{a^2\omega}{\nu}\cos\tau + \nabla^2 w. \tag{2.10}$$

This equation can be seen to be controlled by two parameters, a non-dimensional frequency parameter $\alpha = a(\omega/\nu)^{\frac{1}{2}}$ and an amplitude parameter $G = 2K^2a^3/R\nu^2\omega^2$.

If the pressure gradient amplitude is rewritten as $W_0\omega$, where W_0 is the peak of the instantaneous mean flow, then G becomes equivalent to the Dean expansion parameter. The relationship between W_0 and K becomes more complicated for increasing α but in the low-frequency limit the expansion scheme used is in fact equivalent to Dean's.

The amplitude parameter has the alternative form $2\alpha^2 R_s$. Since the expansion used is to be valid for all α this implies that it is only valid for $R_s \ll 1$. Thus since G is considered small the equations are expanded in terms of G, and collecting terms of equal powers the following equations result.

The expansions

$$w = w_0 + Gw_1 + G^2 w_2 + \ldots$$

and

$$\Psi = G\Psi_1 + G^2\Psi_2 + \ldots$$

give

$$\alpha^2 \frac{\partial w_0}{\partial \tau} - \left(\frac{\partial^2 w_0}{\partial r^2} + \frac{1}{r}\frac{\partial w_0}{\partial r}\right) = \alpha^2 \cos\tau, \tag{2.11}$$

$$\alpha^2 \frac{\partial}{\partial \tau}(\nabla^2\Psi_1) - \nabla^4\Psi_1 = w_0 \cos\phi \frac{\partial w_0}{\partial r}, \tag{2.12}$$

$$\alpha^2 \frac{\partial w_1}{\partial \tau} - \nabla^2 w_1 = \frac{1}{r}\frac{\partial \Psi_1}{\partial \phi}\frac{\partial w_0}{\partial r}, \tag{2.13}$$

$$\alpha^2 \frac{\partial}{\partial \tau}(\nabla^2\Psi_2) - \nabla^4\Psi_2 = \frac{w_0}{r}\left(r\cos\phi\frac{\partial w_1}{\partial r} - \sin\phi\frac{\partial w_1}{\partial \phi}\right) + w_1\cos\phi\frac{\partial w_0}{\partial r} + \frac{1}{r}\left(\frac{\partial \Psi_1}{\partial \phi}\frac{\partial}{\partial r} - \frac{\partial \Psi_1}{\partial r}\frac{\partial}{\partial \phi}\right)\nabla^2\Psi_1. \tag{2.14}$$

3. Solution for arbitrary α

The straight-pipe equation (2.11) was first solved by Sexl (1934) and its solution can be written in the form

$$w_0 = B\cos\tau + (1-A)\sin\tau, \tag{3.1}$$

where

$$B = \frac{\mathrm{bei}\,\alpha\,\mathrm{ber}\,\alpha r - \mathrm{ber}\,\alpha\,\mathrm{bei}\,\alpha r}{\mathrm{bei}^2\alpha + \mathrm{ber}^2\alpha}$$

and

$$A = \frac{\mathrm{bei}\,\alpha\,\mathrm{bei}\,\alpha r + \mathrm{ber}\,\alpha\,\mathrm{ber}\,\alpha r}{\mathrm{bei}^2\alpha + \mathrm{ber}^2\alpha},$$

where ber, bei are the real and imaginary Kelvin's functions. The right-hand side of equation (2.12) may now be evaluated and a solution is suggested of the form

$$\Psi_1 = \Psi_{10}(r,\phi) + \Psi_{12}(r,\phi)\,e^{i2\tau}. \tag{3.2}$$

Substitution of this formulation of the secondary flow into (2.12) leads to

$$\nabla^4\Psi_{10} = \frac{1}{2}\left\{(1-A)\frac{dA}{dr} - B\frac{dB}{dr}\right\}\cos\phi, \tag{3.3}$$

$$2i\alpha^2\nabla^2\Psi_{12} - \nabla^4\Psi_{12} = \frac{1}{2}\left\{B\frac{dB}{dr} + (1-A)\frac{dA}{dr} + i\left[B\frac{dA}{dr} - (1-A)\frac{dB}{dr}\right]\right\}\cos\phi. \tag{3.4}$$

Since the only variation with ϕ on the right-hand side of these equations is via the factor $\cos\phi$, separable solutions of the form

$$\Psi_{10} = \tfrac{1}{2}C_0(r)\cos\phi, \quad \Psi_{12} = \tfrac{1}{2}C_2(r)\cos\phi, \tag{3.5}$$

are sought with the boundary conditions

$$C_0 = C_2 = \frac{dC_0}{dr} = \frac{dC_2}{dr} = 0 \quad \text{at} \quad r = 1. \tag{3.6}$$

The occurrence of the bi-harmonic and Laplacian operators on the left-hand side

of these equations suggest the finite Hankel integral transform may be appropriate to aid a solution. The form of the finite Hankel transform is given by Sneddon (1946) as

$$\bar{C}(\xi_j) = \int_0^1 C(r)\, J_\mu(\xi_j r)\, r\, dr, \tag{3.7}$$

with the inversion formula

$$C(r) = 2 \sum_{j=1}^{\infty} \frac{\bar{C}(\xi_j)\, J_\mu(\xi_j r)}{[J'_\mu(\xi_j)]^2}, \tag{3.8}$$

where μ is the order of the Bessel function and ξ_j is the jth eigenvalue of the equation

$$J_\mu(\xi_j) = 0. \tag{3.9}$$

The first-order Hankel transform involved in this equation cannot be evaluated analytically because of the terms involved on the right-hand side of the equation. The transformed solutions can be evaluated using the Gaussian quadrature scheme of Stroud (1966). Details of the solutions may be found in Mullin (1978).

Thus the stream function Ψ_1 may be obtained and is given by

$$\Psi_1 = \tfrac{1}{2} \cos\phi [C_0 + C_{2\mathscr{R}} \cos 2\tau - C_{2\mathscr{I}} \sin 2\tau], \tag{3.10}$$

where $C_{2\mathscr{R}}$ and $C_{2\mathscr{I}}$ are the real and imaginary parts of C_2 and these together with C_0 may be found from the relevant inversion formulae.

The procedure is repeated for equation (2.13) and the resulting solution for the first-order axial-velocity perturbation together with the appropriate boundary condition is obtained as

$$w_1 = \tfrac{1}{4} \sin\phi [D_{1\mathscr{R}} \cos\tau - D_{1\mathscr{I}} \sin\tau + D_{3\mathscr{R}} \cos 3\tau - D_{3\mathscr{I}} \sin 3\tau]. \tag{3.11}$$

Again $D_{1\mathscr{R}}$, $D_{1\mathscr{I}}$, $D_{3\mathscr{R}}$ and $D_{3\mathscr{I}}$ were evaluated numerically using the appropriate inversion formulae. Because of the nature of the axial-velocity distribution found it was of interest to investigate the effects of this upon the secondary flow. Thus a solution to (2.14) was found using the Hankel transform technique, although the occurrence of the $\sin 2\phi$ factor required the second-order transform. The solution is given by

$$\Psi_2 = \tfrac{1}{8} \sin 2\phi [H_{20} + H_{22\mathscr{R}} \cos 2\tau - H_{22\mathscr{I}} \sin 2\tau + H_{24\mathscr{R}} \cos 4\tau - H_{23\mathscr{I}} \sin 4\tau], \tag{3.12}$$

where the functions H_{20}, $H_{22\mathscr{R}}$, $H_{22\mathscr{I}}$, $H_{24\mathscr{R}}$ and $H_{24\mathscr{I}}$ are evaluated numerically.

The use of the finite Hankel transform involves the evaluation of integrals containing products of Bessel functions and Kelvin functions. The Kelvin functions become large as α increases and thus convergence of the integrals becomes difficult to achieve for large α. In practice, computing time becomes prohibitive for $\alpha \geqslant 11$, when up to 22 terms are required for convergence of the inversion series. In this regime it is therefore more appropriate to adopt the boundary-layer methods first proposed by Lyne (1970).

4. Small α approximation

In order to gain some physical insight into the problem the case is now considered where both G and α are small. The approximate equation obtained by the expansion in terms of G is now expanded in terms of α^2. This allows closed-form analytical solutions to be found.

The straight-pipe solution becomes

$$w_0 = \alpha^2\Big[\tfrac{1}{4}(1-r^2)\cos\tau + \frac{\alpha^2}{64}(3-4r^2+r^4)\sin\tau + \frac{\alpha^4}{64}\cos\tau\left(-\tfrac{19}{36}+\tfrac{3}{4}r^2-\tfrac{1}{4}r^4+\frac{r^6}{36}\right) + \frac{\alpha^6}{256}\sin\tau\left(-\tfrac{53}{144}+\tfrac{19}{36}r^2-\tfrac{3}{16}r^4+\frac{r^6}{36}-\frac{r^8}{576}\right)+O\{\alpha^8\}\Big]. \quad (4.1)$$

The first term in the series shows that for very small frequencies the velocity profile is parabolic and in phase with the applied pressure gradient. The next term arises owing to the first-order effects of inertia in the central region of the flow. The final two terms in the series show that as α increases then for a fixed pressure gradient amplitude there will be a decrease in the axial velocity. A comparison between the exact solution and the approximate solution shows that this expansion breaks down rapidly for $\alpha \geqslant 1{\cdot}5$.

Using this approximate solution, closed-form expressions for the first-order secondary-flow equations are obtained:

$$\Psi_1 = \alpha^4\{F_0(r)\cos^2\tau + \alpha^2 F(r)\sin 2\tau + \alpha^4[F_1(r)+F_2(r)\cos 2\tau] + \alpha^6 F_3(r)\sin 2\tau + O(\alpha^8)\}\cos\phi. \quad (4.2)$$

The function $F_0(r)$ is equivalent to that found in the steady-flow solution of Dean and its time dependency is as one would expect intuitively. The functions $F_0(r)-F_3(r)$ are shown in figure 2. They all have the same form except $F_2(r)$, which has a peak near the axis of the tube and reverses sign near the wall. This gives the first indication of the type of secondary flow found in the boundary-layer work of Lyne.

A closed-form solution can now be found to the first-order axial-velocity perturbation equation (2.13):

$$w_1 = \alpha^6\sin\phi[F_4(r)\cos^3\tau + \alpha^2 F_5(r)\sin\tau\cos^2\tau + \alpha^4(F_6(r)\cos\tau + F_7(r)\cos^3\tau) + \alpha^6(F_8(r)\sin\tau + F_9(r)\sin\tau\cos^2\tau) + O\{\alpha^8\}]. \quad (4.3)$$

The function $F_4(r)$ is equivalent to that solution found by Dean for the steady-flow case but now, owing to the time dependency, the perturbation will be very small over the periods 60°–120° and 240°–300° in the pressure cycle. Thus as α increases the higher-order terms may have appreciable effects within this range.

The functions $F_4(r)-F_9(r)$ are shown in figure 3. They are similar in form, except $F_8(r)$, which has its maximum towards the centre of the tube. Further, the function $F_7(r)$ indicates that for larger values of α the perturbation may change sign at the 0° phase position.

5. Results and discussion

In the quasi-steady limit the secondary-flow streamline patterns ought to be in agreement with the steady-flow results on McConalogue & Srivastava (1968) and Collins & Dennis (1975). Both of these studies used the limit of Dean's work as their starting-point and it is of interest to see how the results for $\Psi_{\max}$, the maximum value of the secondary-flow stream function, compare for various Dean numbers. $G = 9216$ is equivalent to the limiting value of Dean's expansion parameter, which was 576.

The results presented in table 1 are for phase 0° using the Hankel transform solution.

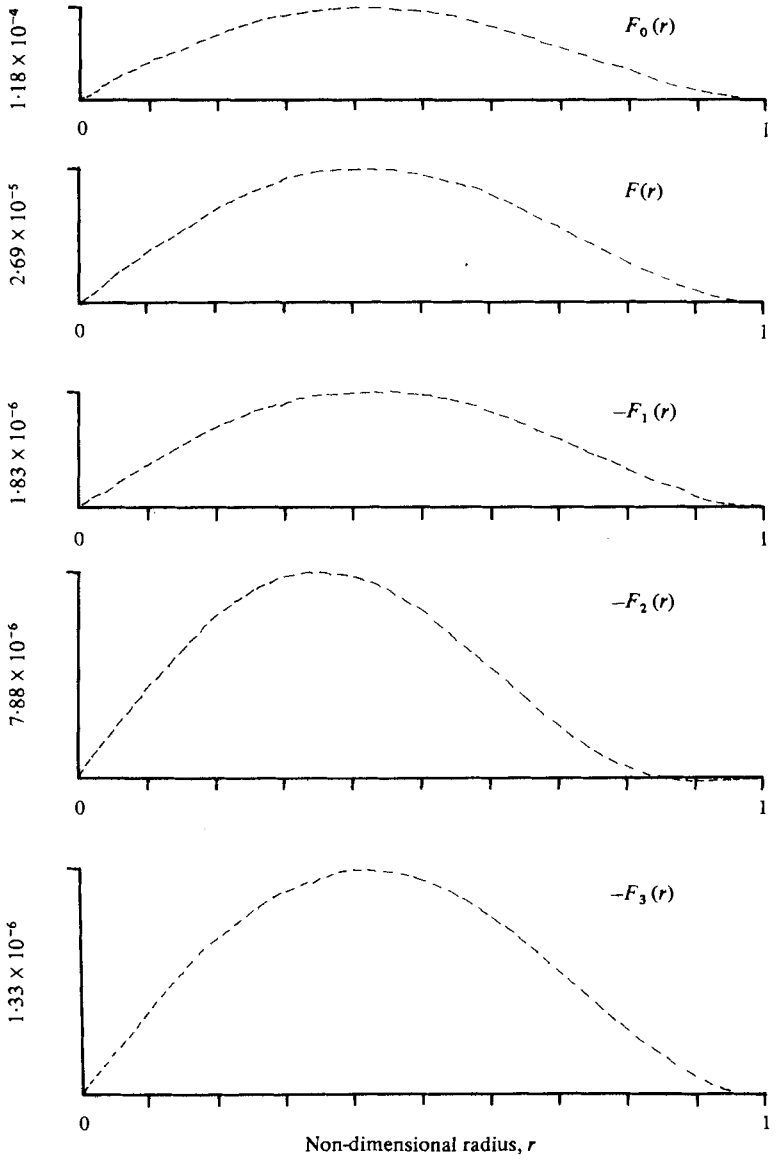

FIGURE 2. Functions $F_0(r) - F_3(r)$ associated with small-α secondary-flow approximation plotted to show radial dependence.

Thus reasonable agreement is obtained at the Dean limit, but the results presented here indicate that this is also the limit of this expansion. The secondary-flow streamline pattern is shown in figure 4 in which the pattern is very similar to the one presented by McConalogue & Srivastava for the same value of G.

The nature of the time dependency of the secondary flow in the central area of the tube was investigated experimentally and the results are shown in figure 5. The reference velocity used in the normalization was the peak radial velocity measured in the centre of the tube and the value of G was 21·58. The secondary flow is directed outwards

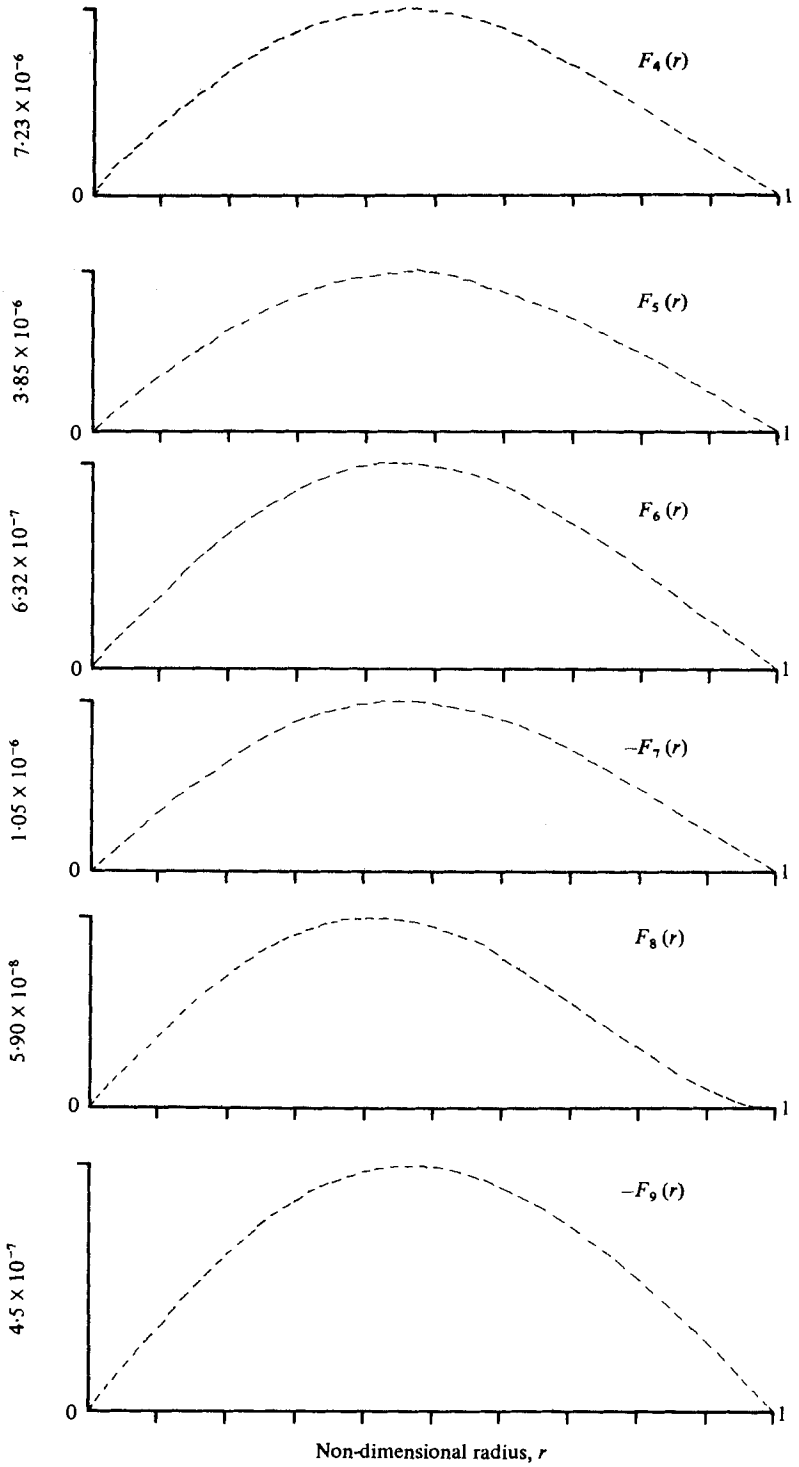

FIGURE 3. Functions $F_4(r) - F_9(r)$ associated with small-α axial-velocity perturbation approximation plotted to show radial dependence.

	G	Ψ_{max}	G	Ψ_{max}
McConalogue & Srivastava (1968)	9216	0·95	14607·14	1·36
Collins & Dennis (1975)	9216	0·99	—	—
Present	9216	0·968	14607·14	1·21

TABLE 1

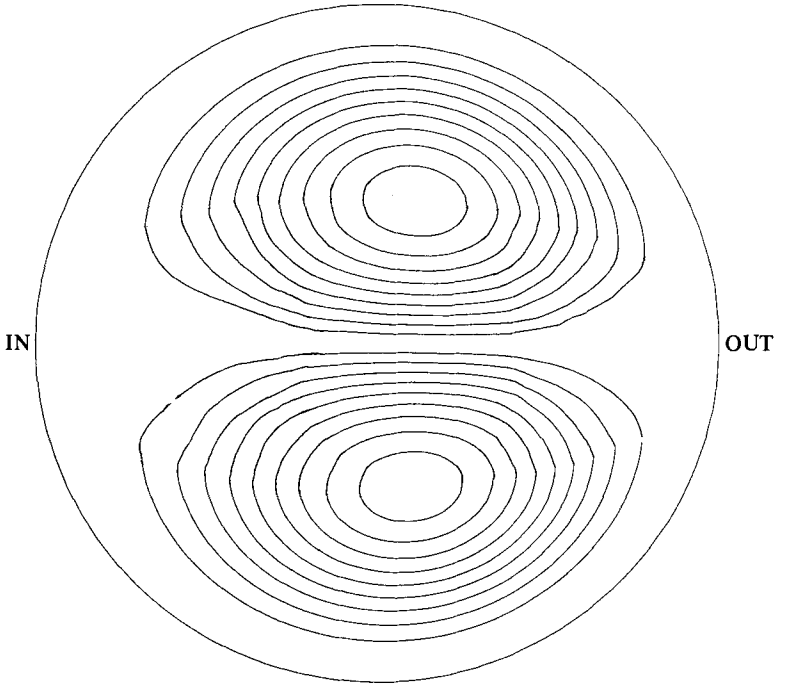

FIGURE 4. Secondary-flow streamlines for the case $\alpha = 1$, $G = 9216$, $\psi = 0{\cdot}1$–$0{\cdot}9$ and phase position 0°.

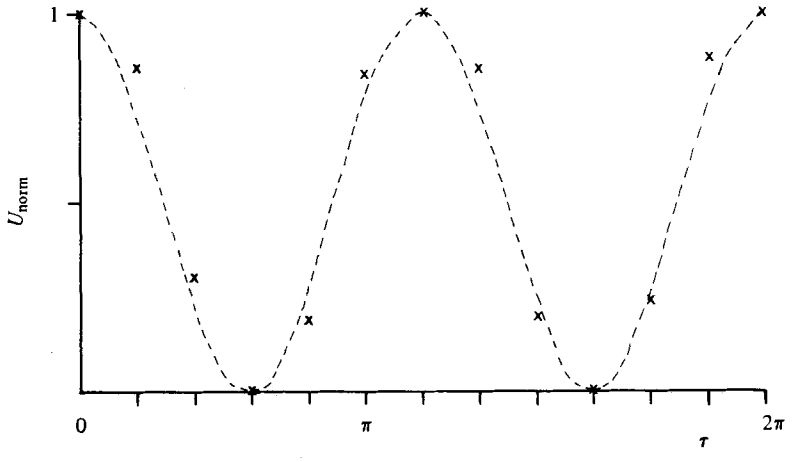

FIGURE 5. Normalized secondary flow measured in the central plane of the bend wall with $\alpha = 0{\cdot}84$. ×, measured points; – – –, theoretical curve obtained from equation (4.2).

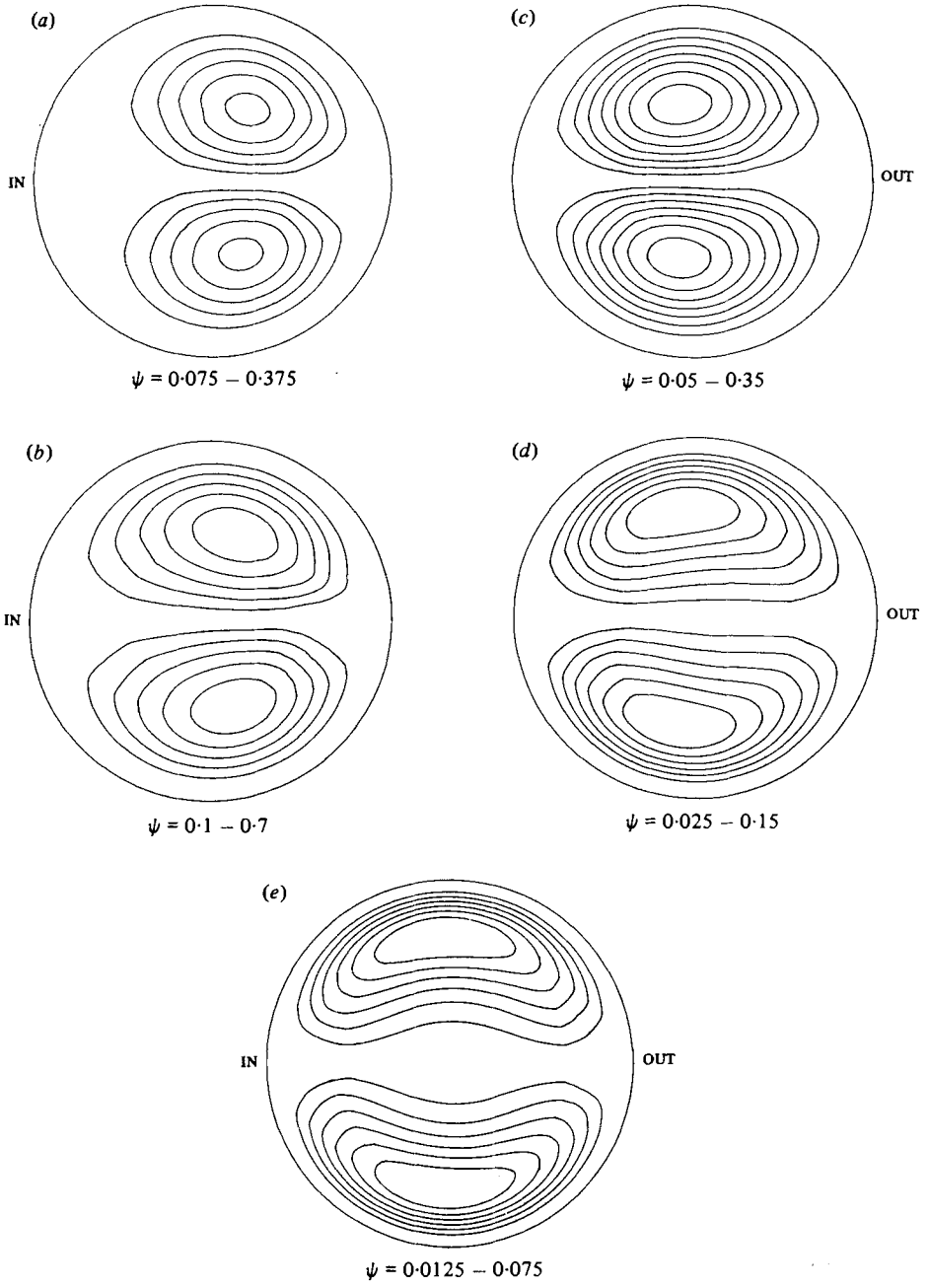

FIGURE 6. Steady component of secondary flow with fixed $G = 300$. (*a*) $\alpha = 2$, $\psi = 0{\cdot}075$–$0{\cdot}375$; (*b*) $\alpha = 4$, $\psi = 0{\cdot}1$–$0{\cdot}7$. (*c*) $\alpha = 6$, $\psi = 0{\cdot}05$–$0{\cdot}35$; (*d*) $\alpha = 8$, $\psi = 0{\cdot}025$–$0{\cdot}15$; (*e*) $\alpha = 10$, $\psi = 0{\cdot}0125$–$0{\cdot}075$.

from the centre of curvature and behaves as $\cos^2\tau$ in agreement with the quasi-steady approximation.

It is of interest now to see how the steady secondary-flow streamline pattern varies with α for a fixed value of G. This is shown in figure 6, which demonstrates the gradual

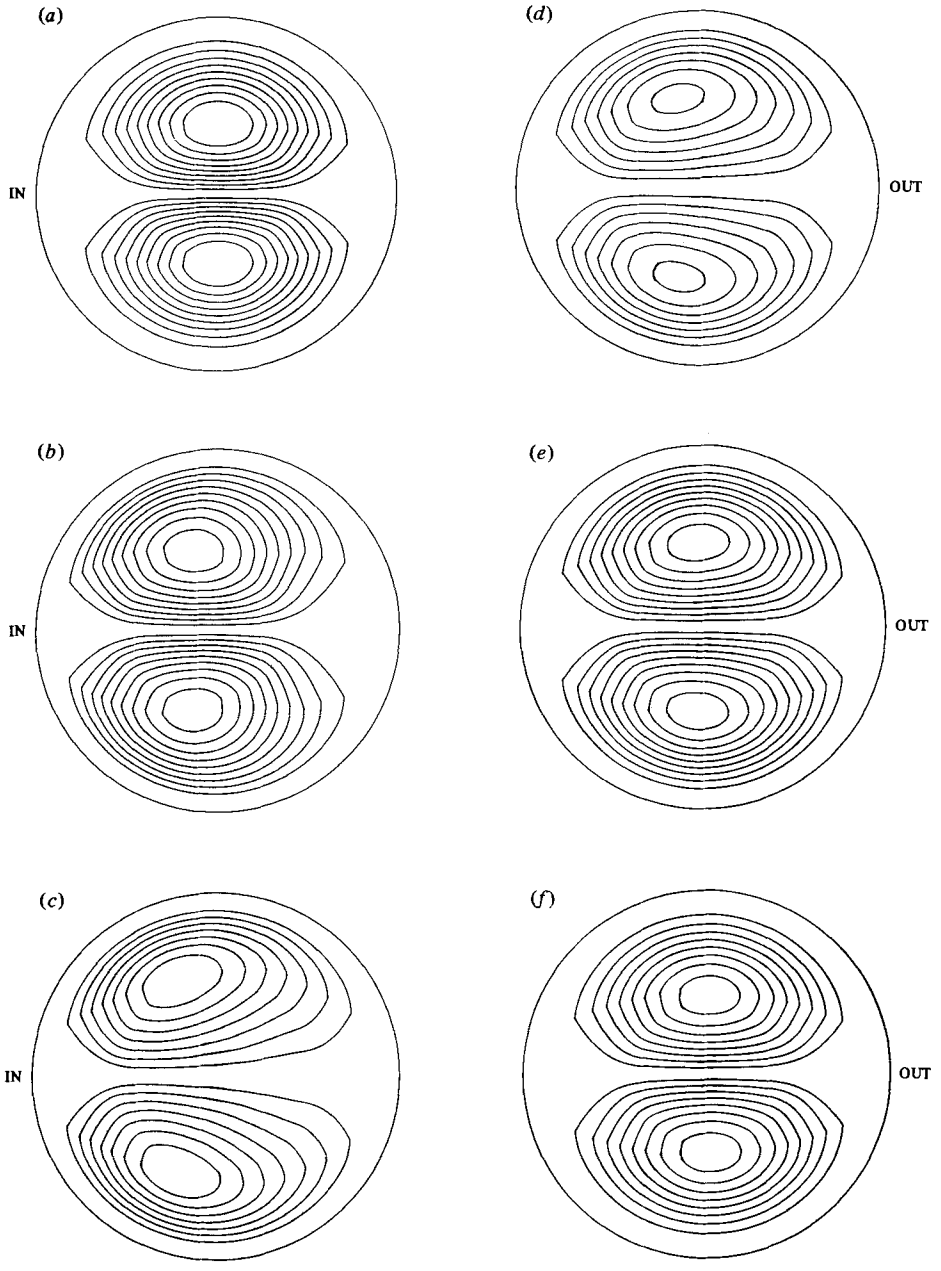

FIGURE 7. Secondary-flow streamlines for the case $\alpha = 5$, phase positions 0°–150° with $G = 300$. Phase positions: (*a*) 0°; (*b*) 30°; (*c*) 60°; (*d*) 90°; (*e*) 120°; (*f*) 150°.

development of a stagnation region in the centre of the tube with increasing α. Two additional vortices are finally produced in this central region which rotate in the opposite direction to the main wall vortices, and the four-vortex system found by Lyne appears. The α value at which this transition occurs is found to be approximately 11·0, which is slightly lower than the value found by Lyne. This discrepancy occurs because the approximations presented in this study are only equivalent to the first-

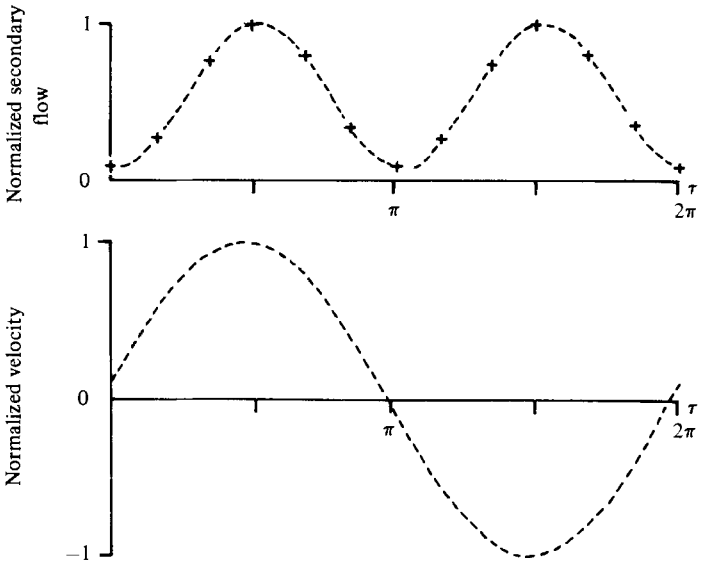

FIGURE 8. Normalized secondary flow and velocity plots for the tube centre when $\alpha = 4{\cdot}36$. Experimental secondary flow measurements made at $D = 42{\cdot}84$.

order approximation of Lyne (Mullin 1978). The next term in the series contains a correction for large α.

Another feature of the steady-secondary-flow streamline patterns is the change in direction of the displacement of the centres of the vortices for increasing α. When $\alpha = 2$ and 4 they are displaced towards the outside of the bend to produce patterns similar to those of McConalogue & Srivastava (1968). As α increases to 6 the centres move towards the inside of the bend and remain there at $\alpha = 10$. This thickening of the vortex core on the inside of the curve was attributed to finite-curvature effects by Bertelsen (1975), but from these results it would appear to depend on G when $\alpha \geqslant 6$.

The full time-dependent streamlines for $\alpha = 5$ are shown in figure 7. The centres of the vortices remain displaced towards the inside of the bend until phase position 120°. The stagnation region is present at the 60° and 90° phase positions and at the 120° and 150° positions the outward streaming becomes uniform in the centre of the tube, and is similar to that found in the quasi-steady region. Thus at this α value all the elements of the secondary-flow pattern appear in one cycle. The time dependency of the secondary flow was investigated experimentally near this α value and the results are shown in figure 8. Thus the secondary flow is directed outwards at all phase positions and remains in phase with the central axial velocity component.

If now the α value is increased to 10 then the patterns shown in figure 9 are obtained. The stronger main vortices are slightly thicker towards the inside of the curve at all phase positions. The stagnation zone in the centre of the tube is prominent and, at 33° phase, twin vortices rotating in the opposite direction to the main vortices appear. Even at phase position 80° where the strongest inner vortices occur, it is clear that they occupy only a small area of the centre of the tube. Thus the situation portrayed by the boundary-layer work of Lyne (1970) is only reached very gradually as α increases.

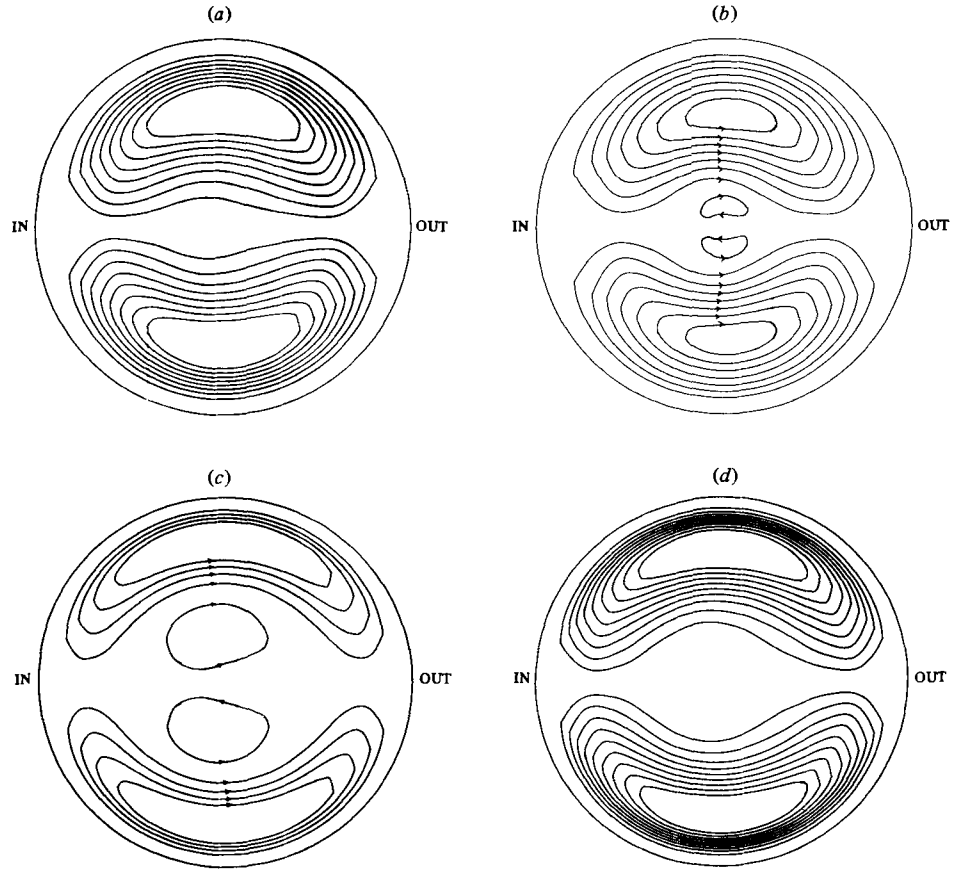

FIGURE 9. Secondary-flow streamline patterns obtained when $\alpha = 10$ and $G = 200$. (*a*) Phase position 120°, $\Psi = 0{\cdot}005$–$0{\cdot}021$; (*b*) Phase position 33°, $\Psi = 0{\cdot}005$–$0{\cdot}035$, $-0{\cdot}0005$; (*c*) Phase position 80°, $\Psi = 0{\cdot}01$–$0{\cdot}04$, $-0{\cdot}005$; (*d*) Phase position 0°, $\Psi = 0{\cdot}01$–$0{\cdot}08$.

From this theoretical study it may therefore be concluded that the secondary flow is of similar form over most of the alpha range until the boundary-layer-type region is reached. There is a gradual development of a reverse secondary flow which originates from the centre of the tube when $\alpha \geqslant 10$.

Theoretical and experimental axial-velocity profiles for fully developed oscillatory flow in a curved pipe are now presented. The theoretical results were obtained using the Hankel transform solutions and the experimental results are presented for both $\frac{1}{50}$th and $\frac{1}{7}$th curvature pipes. The profiles were mainly measured in the plane of the bend at stations 90° round the $\frac{1}{7}$th curve and 180° round the $\frac{1}{50}$th curve from the inlet, where it was assumed that essentially fully developed conditions occurred. This point was investigated in detail experimentally and the results are presented in part 1 (Mullin & Greated 1980) of this paper.

The experimental velocity profiles presented were obtained at fixed phase positions in the pressure cycle using a sampling technique. The one shown in figure 10 was obtained in the quasi-steady region. The experimental measurement was made at 0° phase position, $\alpha = 0{\cdot}99$ and peak $D = 12$ (where peak $D \equiv (2W_0 a/\nu)(a/R)^{\frac{1}{2}}$), in

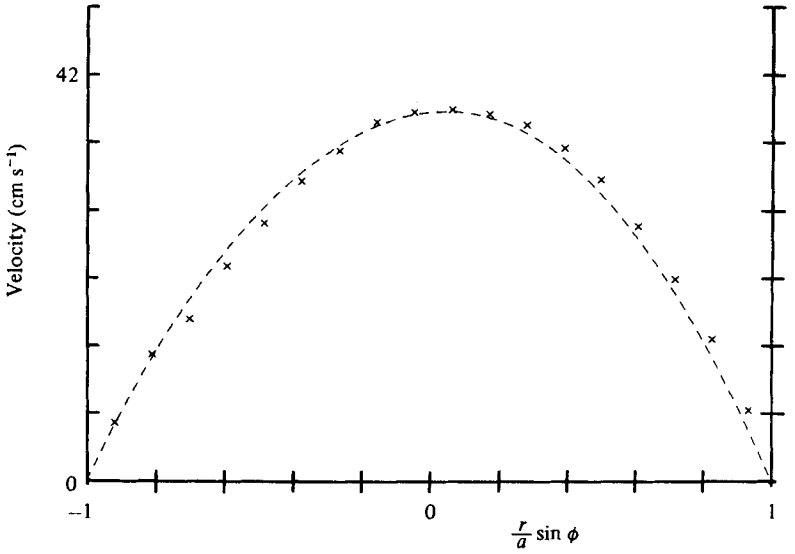

FIGURE 10. Comparison between experiment and theory in the quasi-steady flow region with $D = 12, a/R = 1/50$, phase position 0°, $\alpha = 0{\cdot}99$. Crosses give experimental points and theoretical profile obtained using the results of the small-α approximation.

the $\frac{1}{50}$th curved tube. There is only a small departure from the Poiseuille flow distribution and comparison between theory and experiment is found to be good.

The effect of increasing α to 2·56 is illustrated in figure 11, where comparison between theory and experiment is also made. (It should be noted here that all velocity profiles have been plotted irrespective of direction of the flow for convenience.) The experimental measurements were made in the tube of curvature $\frac{1}{50}$th and the peak $D = 9{\cdot}53$. The experimental results are just outside the expected limits of the theory (see Mullin 1978 for details) but, as can be seen, the agreement is found to be good. At 150° and 180° phase positions in the pressure cycle, the higher axial-velocity components feature towards the inside of the curve, whereas, at the 60° and 120° positions, the peak in the profile is found towards the outside of the curve, as in the quasi-steady case.

A further increase in α to 4·36 gives the velocity profiles shown in figure 12. The higher axial-velocity components are now found nearer the inside of the curve for a greater portion of the cycle. These measurements were made in the $\frac{1}{7}$th curved tube and this is a possible explanation for the more marked distortion in the experimental profiles. However, the agreement between theory and experiment is reasonable. Further experimental measurements were made in the $\frac{1}{50}$th curved tube at a slightly lower α value and agreement between theory and experiment is found to be good. These results, together with other experimental results mainly confirming the above findings, are contained in Mullin (1978).

In order to gain further insight into the behaviour of the axial velocity over the transition region, non-dimensionalized velocity–time diagrams for two positions in the flow, viz. $0{\cdot}1r$ and $0{\cdot}9r$, are shown in figures 13 and 14, in the form axial-velocity perturbation plus corresponding straight pipe axial-velocity component for α values 2, 5, 7, and 10.

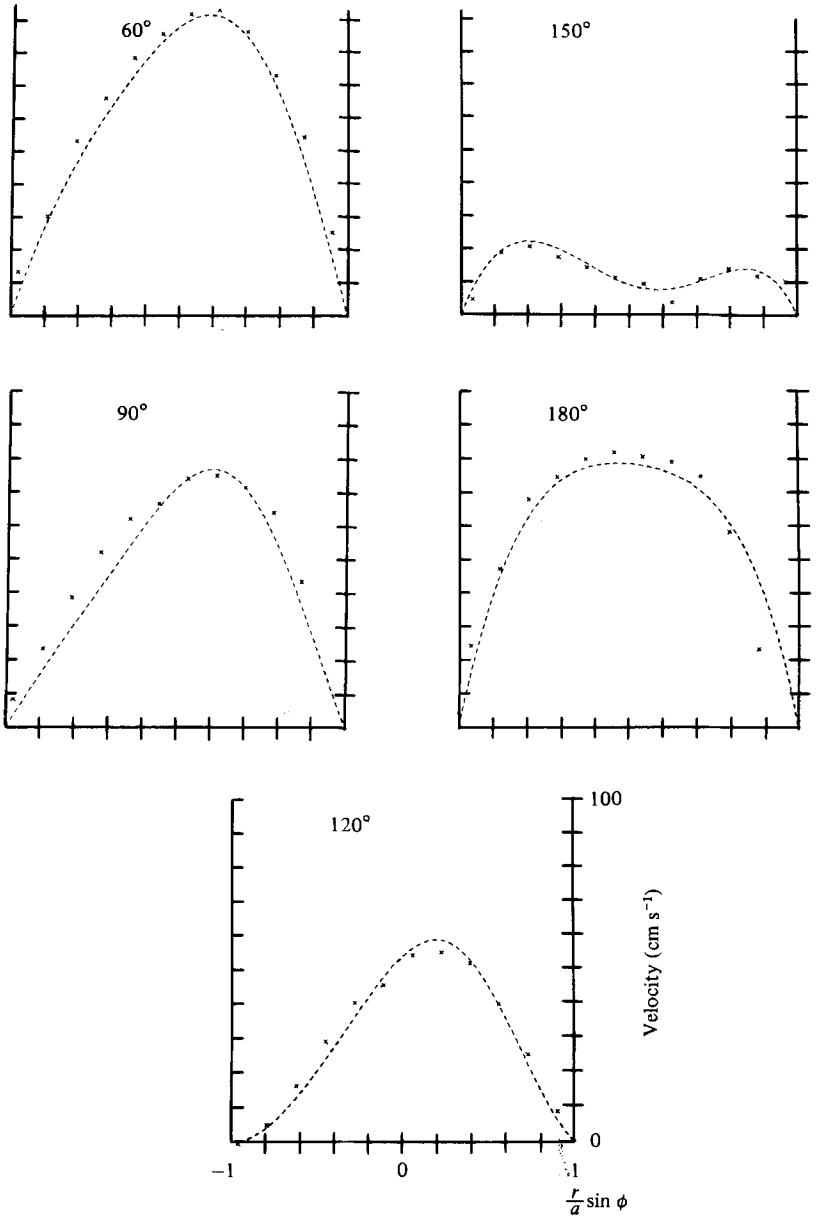

FIGURE 11. Comparison between theory and experiment for axial-velocity flow profiles measured in the plane of the bend with $\alpha = 2{\cdot}56$, peak $D = 9{\cdot}53$, $a/R = 1/50$ and phase positions 60°–180°. All profiles are plotted to the same scale.

At $\alpha = 2$ the effect of the $\cos^3\tau$ term found in the quasi-steady approximation, is still dominant and the beginnings of the reversal of the direction of action of the perturbation can be seen. Between $\alpha = 2$ and 5, a phase lag develops across the straight-pipe flow, while the perturbations remain in phase with each other. Also the phase lag between the perturbations and the applied pressure gradient develops rapidly and approaches a factor of two times the corresponding phase lag between

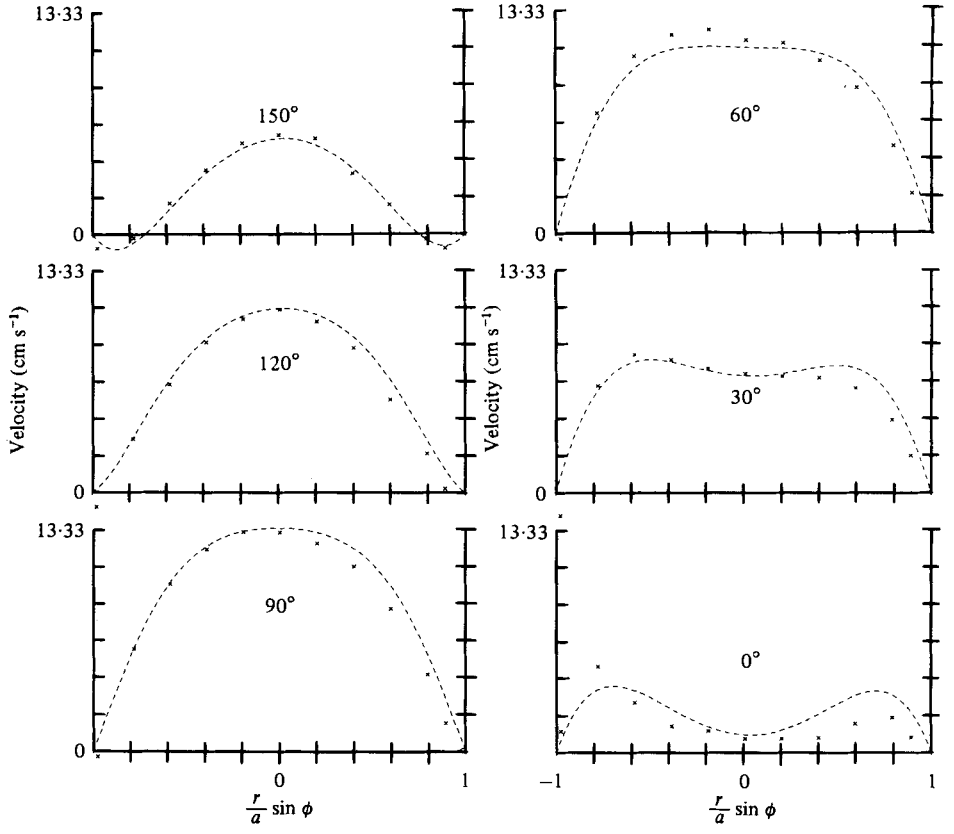

FIGURE 12. Velocity profiles for phase positions 0°–150° with $\alpha = 4{\cdot}36$, peak $D = 9{\cdot}98$ and $a/R = \frac{1}{7}$. Theoretical profile derived using equations (3.11) and (3.1).

the straight-pipe component and the pressure gradient. Thus the perturbation acts almost in anti-phase with the main flow at $\alpha = 5$.

Above $\alpha = 5$ the phase difference across the straight pipe remains fixed but now the perturbations move out of phase with each other. The perturbation at the wall remains in anti-phase with the main flow but the one in the centre of the tube moves back into phase with the main flow. Thus for large values of α the axial velocity distribution will be such that the higher axial-velocity component will feature towards the inside of the curve at all phase positions close to the wall.

The main conclusions of this study are that the general structure of the secondary flow in the limits $\alpha \to 0$ and $\alpha \to \infty$ is similar to that found in previous theoretical and experimental studies. The transition region from the quasi-steady to the large-α state may be thought of as a gradual development of a stagnation region in the centre of the tube, as the centrifugally generated secondary flow, associated with the viscous flow, is confined to regions near the wall with increasing α. Eventually, where α becomes large, inward centrifuging occurs in the central flow region.

The effect of the secondary flow on the axial flow is to cause the axial-velocity profile peak to be displaced towards the outside of the curve in the quasi-steady region and to the inside of the curve in the large-α region. It therefore seems plausible that in the transition stage between these two states both effects will be found. However, it

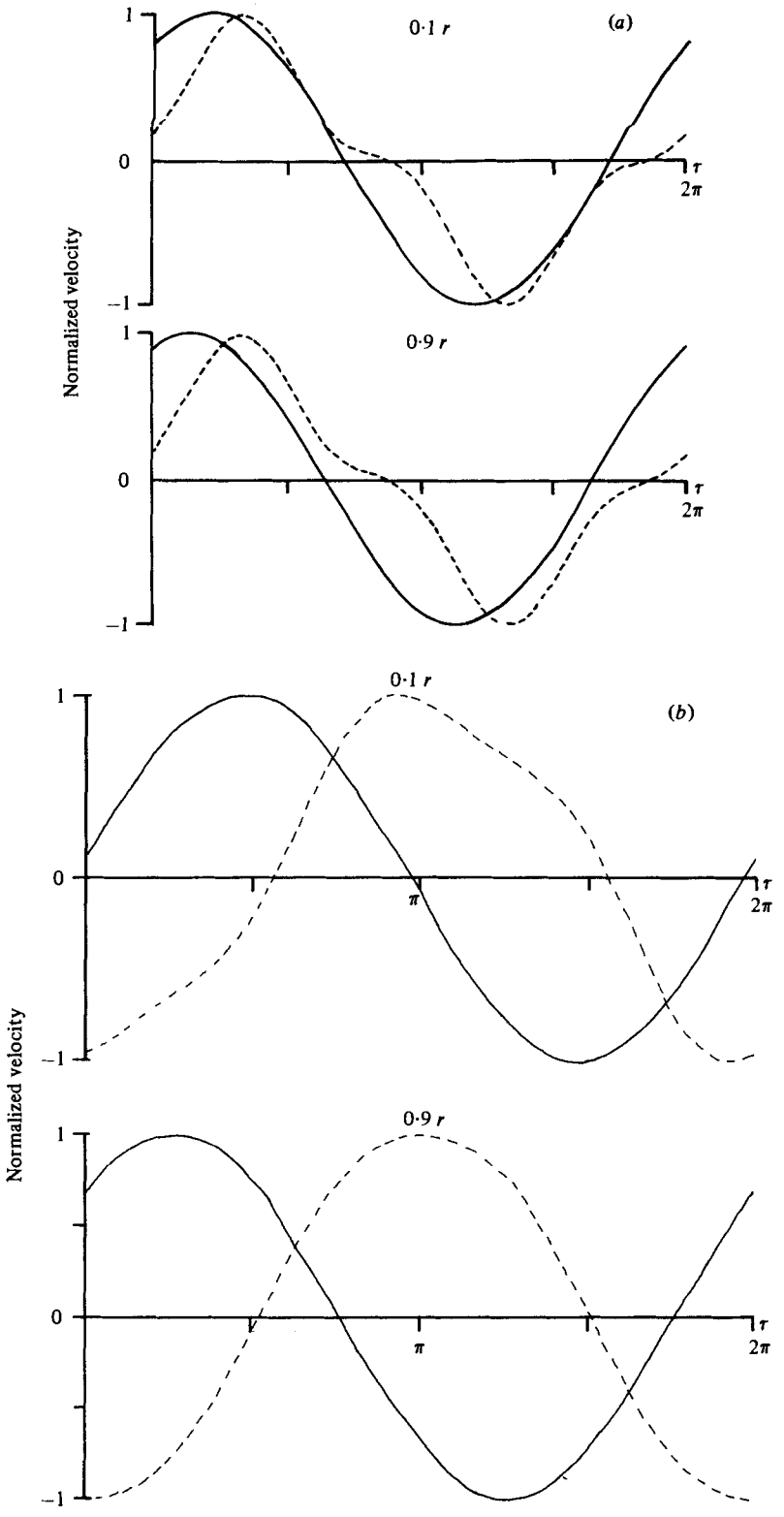

FIGURE 13. Normalized velocity–time diagrams for straight-pipe flow (——), and first-order perturbation due to curvature (– – –) for radial positions $0{\cdot}1r$ and $0{\cdot}9r$ for (*a*) $\alpha = 2$ and (*b*) $\alpha = 5$.

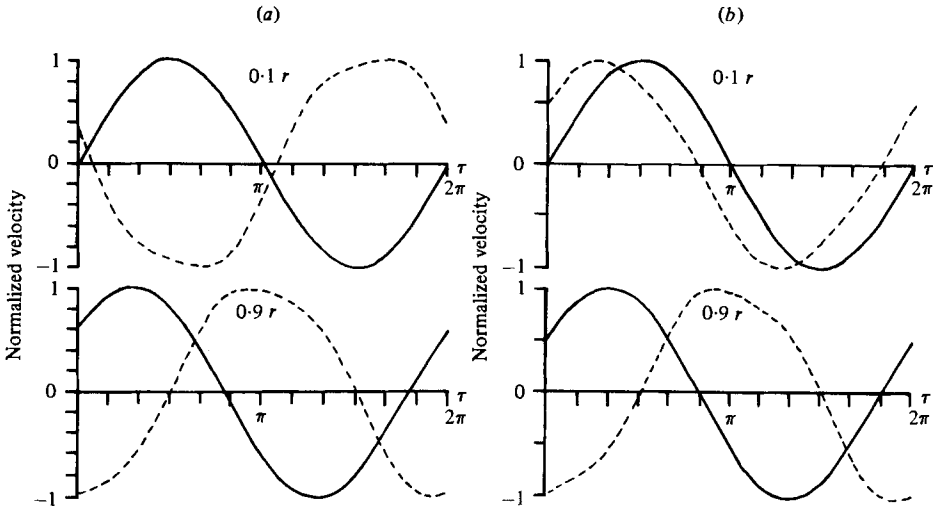

FIGURE 14. Normalized velocity–time diagrams for straight-pipe flow (——) and first-order perturbation due to curvature (– – –) for radial positions $0{\cdot}1r$ and $0{\cdot}9r$ for (*a*) $\alpha = 7$ and (*b*) $\alpha = 10$.

would appear that the accepted physical model used to explain the interaction between the secondary flow and the axial velocity is not sufficient to explain the effects found in this study in the transition stage where outward-flowing secondary flow in the centre of the tube is accompanied by the maximum of the axial-velocity distribution positioned at the inside of the bend.

T. Mullin acknowledges the support of the S.R.C. during the period of this research.

REFERENCES

BERTELSEN, A. F. 1974 An investigation of the oscillating viscous flow in a curved pipe with special emphasis on low Reynolds number secondary steady streaming effects. *Univ. of Bergen, Norway, Rep.* no. 67.

BERTELSEN, A. F. 1975 An experimental investigation of low Reynolds number secondary streaming effects associated with an oscillating viscous flow. *J. Fluid Mech.* **70**, 519–527.

BLENNERHASSET, P. J. 1976 Secondary motion and diffusion in unsteady flow in a curved pipe. Ph.D. thesis, Imperial College, London.

COLLINS, W. M. & DENNIS, S. C. R. 1975 The steady motion of a viscous fluid in a curved tube. *Quart. J. Mech. Appl. Math.* **28**, 133–156.

DEAN, W. R. 1928 The stream-line motion of fluid in a curved pipe. *Phil. Mag.* **5** (7), 673–695.

LYNE, W. H. 1970 Unsteady viscous flow in a curved pipe. *J. Fluid Mech.* **45**, 13–31.

MCCONALOGUE, D. J. & SRIVASTAVA, R. S. 1968 Motion of a fluid in a curved tube. *Proc. Roy. Soc.* A 37–53.

MULLIN, T. 1978 Oscillatory flow in curved tubes. Ph.D. thesis, University of Edinburgh.

MULLIN, T. & GREATED, C. A. 1980 Oscillatory flow in curved pipes. Part 1. The developing-flow case. *J. Fluid Mech.* **98**, 383–395.

MUNSEN, B. R. 1975 Experimental results for oscillating flow in a curved pipe. *Phys. Fluids* **18**, 1607–1609.

MUNSEN, B. R. 1976 Secondary flows in a slowly oscillating torus. *Phys. Fluids* **19**, 1823–1825.

SEXL, T. 1930 Über den von E. G. Richardson entdeckten 'Annulareffeckt'. *Z. Phys.* **61**, 349–362.

SMITH, F. T. 1975 Pulsatile flow in curved pipes. *J. Fluid Mech.* **71**, 15–42.

SNEDDON, I. N. 1946 Finite Hankel transforms. *Phil. Mag.* **37** (0), 17–25.

STROUD, A. H. 1966 *Gaussian Quadrature Formulae*. Englewood Cliffs, New Jersey: Prentice-Hall.

ZALOSH, R. G. 1970 Pulsating flow in a curved tube. Ph.D. thesis, North Eastern University, Boston.

ZALOSH, R. G. & NELSON, W. G. 1973 Pulsating flow in a curved tube. *J. Fluid Mech.* **59**, 693–705.